J. Fluid Mech. (2005), *vol.* 540, *pp.* 353–371.
doi:10.1017/S0022112005006014 Printed in the United Kingdom

Vibrational thermocapillary instabilities

By ABDELFATTAH ZEBIB

Mechanical & Aerospace Engineering, Rutgers University, Piscataway, NJ 08865, USA

(Received 14 January 2005 and in revised form 6 May 2005)

We study vibrational instabilities of the thermocapillary return flow driven by a constant temperature gradient along the free surface of an infinite layer that vibrates in its normal direction with acceleration of amplitude g_1 and frequency ω_1. The layer is unstable to hydrothermal waves in the absence of vibrations beyond a critical Marangoni number M. Modulated gravitational instabilities with $M=0$ are also possible beyond a critical Rayleigh number R based on g_1. We employ two-time-scale high-frequency asymptotics to derive the equations governing the mean field. The influence of vibrations on the hydrothermal waves is found to be characterized by a dimensionless parameter G that is proportional to R^2. The return flow at $G=0$ is also a mean field basic flow and we study its linear instability at different Prandtl numbers P. The hydrothermal waves are stabilized with increasing G and reverse their direction of propagation at particular values of G that decrease with increasing P. At finite frequencies, a time-periodic base state exists and we study its linear instability by calculating the Floquet exponents. The stability boundaries in the (R, M)-plane are found to be composed of two intersecting branches emanating from the points of pure thermocapillary or buoyant instabilities. Three-dimensional modes are always preferred and the region of stability, while anchored at the point of hydrothermal waves corresponding to $R=0$, is found to grow without bound along the R-axis with increasing frequencies. Results from the two approaches are shown to be in asymptotic agreement at large frequencies.

1. Introduction

Buoyant instabilities can be driven in a quiescent fluid layer owing to density variation with temperature by applying a temperature gradient in a gravitational field. In analogy with an inverted pendulum stabilized by oscillating its pivot, unstable/stable density stratifications can be stabilized/destabilized by vibrating the layer. Gresho & Sani (1970) and Gershuni & Zhukhovitskii (1976) demonstrated these effects in their studies of modulated Rayleigh–Bénard convection. There are also several studies of other modulated buoyant instabilities. Wheeler *et al.* (1991) considered the Rayleigh–Bénard and directional solidification problems and Murray *et al.* (1993) included thermosolutal effects. Farooq & Homsy (1996) and Chen & Chen (1999) investigated side-heated vertical slots. These studies and others referenced therein elucidated the parametric excitation of instabilities via Floquet theory as well as the methods of averaging and multiple time scales to study the phenomena at high frequencies.

Thermocapillary flows can be driven in a fluid layer owing to surface tension variation with temperature by applying a temperature gradient along its interface. Smith & Davis (1983) showed that the thermocapillary return flow of Birikh (1966) is susceptible to hydrothermal wave instabilities in the absence of gravity at some critical

value of the Marangoni number M that is a function of the Prandtl number P. These three-dimensional oblique waves were found to propagate against the direction of the free-surface flow at an angle that is P dependent. Because this return flow induces a temperature gradient in the direction normal to the layer, buoyant instabilities can be excited if the layer is vibrated or equivalently in the presence of a modulated gravitational acceleration. This buoyant instability can be triggered in the part of the cycle when the temperature stratification is unstable. Alternatively, the stable part of the cycle can stabilize the thermocapillary mode.

Suresh & Homsy (2001, hereinafter referred to as SH) investigated the combined buoyant–thermocapillary instability in a fluid layer heated along its interface in the presence of a zero mean time harmonic gravitational acceleration normal to the layer. They showed that either pure thermocapillary or buoyant instabilities are possible. The latter instability, characterized by a Rayleigh number R based on the amplitude of modulation, occurs because modulation induces temperature stratification normal to the layer even with $M = 0$. They found regions in the (R, M)-plane where the two instability mechanisms either reinforced or opposed each other, while shear-driven inflectional instabilities were not important. Their study, however, was limited to two-dimensional situations, and the combined mechanisms of instability were examined at a single frequency.

Because the hydrothermal waves are known to be three-dimensional, we re-examine the problem and allow for three-dimensional instabilities. We show that the preferred purely buoyant instabilities are also three-dimensional. We first carry out an asymptotic analysis valid for large frequencies similar to those in Wheeler *et al.* (1991), Gershuni *et al.* (1997), and Zebib (2001) who studied the influence of vibrations or gravity modulation on several buoyantly unstable problems. The resulting system is simpler to solve than the full problem at finite frequencies that we study next by computing the Floquet exponents. The two approaches are shown to agree asymptotically, with the former computationally efficient in providing more information at the high frequencies thought to be relevant to space experiments.

2. Mathematical model

We consider a horizontal infinite constant property Boussinesq fluid layer of depth d with one bounding surface rigid and the other, where a constant temperature gradient $-B$, $B > 0$, is imposed, free and assumed non-deformable. The surface tension σ^* varies linearly with the temperature T^* (starred quantities are dimensional) according to $\sigma^* = \sigma_r - \gamma(T^* - T_r)$ where a subscript r designates a reference quantity and $T_r = Bd$. We choose the scales d, $\gamma T_r/\mu$, $\mu/\gamma B$, T_r, $\gamma T_r/d$ for length, velocity, time, temperature and pressure, respectively, where ν is the kinematic viscosity, ρ is the density and μ is the dynamic viscosity. The motion is referred to a Cartesian frame of reference attached to the layer that vibrates relative to an inertial frame with acceleration $-g_1 \cos(\omega_1 t^*)\hat{\boldsymbol{n}}$ which contributes the only body force in this otherwise zero-gravity model. Thus the non-dimensional equations of motion are

$$\begin{aligned} \nabla \cdot \boldsymbol{v} &= 0, \\ \frac{M}{P}\frac{\mathrm{D}\boldsymbol{v}}{\mathrm{D}t} &= -\nabla p + \nabla^2 \boldsymbol{v} + \frac{R}{M} T \cos(\omega t)\hat{\boldsymbol{n}}, \\ M\frac{\mathrm{D}T}{\mathrm{D}t} &= \nabla^2 T, \end{aligned} \tag{1}$$

In (1), $\mathrm{D}/\mathrm{D}t = \partial/\partial t + \boldsymbol{v}\cdot\nabla$, $\boldsymbol{v}$ is the velocity vector, p is the modified pressure, $M = \gamma T_r d/\mu\kappa$, $R = g_1\alpha_T T_r d^3/\kappa\nu$, $P = \nu/\kappa$, and κ is the thermal diffusivity. Both top and bottom surfaces are assumed adiabatic and thus the boundary conditions are taken as:

$$\left.\begin{array}{lll} u = v = w = \partial_z T = 0 & \text{on} & z = 0, \\ \partial_z u + \partial_x T = \partial_z v + \partial_y T = w = \partial_z T = 0 & \text{on} & z = 1, \\ T = -x & \text{on} & z = 1. \end{array}\right\} \tag{2}$$

The dimensionless frequency $\omega = \omega_1 d^2/\kappa M$ is arbitrary.

3. Asymptotic solutions at high frequency

The fluid layer is unstable to oblique hydrothermal waves in the absence of modulation. We first investigate the influence of high-frequency vibrations on these thermocapillary instabilities. We also assess whether this approach is also applicable to the pure buoyant instabilities driven entirely by the modulation.

3.1. *Equations of the mean field*

Here we develop the model in the limit $\omega \to \infty$. We might employ the averaging method of Gershuni *et al.* (1997) or two time-scale analysis as in Wheeler *et al.* (1991) and Zebib (2001). We introduce the fast time $\tau = \omega t$ and write

$$\left.\begin{array}{l} \boldsymbol{v} = \bar{\boldsymbol{v}}(\boldsymbol{x}, t) + \tilde{\boldsymbol{v}}(\boldsymbol{x}, t, \tau), \\ p = \bar{p}(\boldsymbol{x}, t) + \tilde{p}(\boldsymbol{x}, t, \tau), \\ T = \bar{T}(\boldsymbol{x}, t) + \dfrac{1}{\omega}\tilde{T}(\boldsymbol{x}, t, \tau), \\ \dfrac{\partial}{\partial t} = \omega\dfrac{\partial}{\partial \tau} + \dfrac{\partial}{\partial t}, \end{array}\right\} \tag{3}$$

where the slowly varying averaged quantities are denoted with an overbar and the rapidly varying 2π periodic functions of τ with a tilde. We further assume asymptotic expansions for both slow and fast variables, substitute in (1), and integrate with respect to τ over one period of 2π. With the tilde variables having zero mean, this gives the leading-order equations in $1/\omega$ for the mean field that when subtracted from the full equations gives the leading equations for the fluctuating quantities as

$$\left.\begin{array}{l} \nabla\cdot\tilde{\boldsymbol{v}} = 0, \\ \dfrac{M}{P}\dfrac{\partial\tilde{\boldsymbol{v}}}{\partial\tau} = -\dfrac{1}{\omega}\nabla\tilde{p} + \dfrac{R}{\omega M}\cos(\tau)\bar{T}\hat{\boldsymbol{n}}, \\ M\dfrac{\partial\tilde{T}}{\partial\tau} = -\tilde{\boldsymbol{v}}\cdot\nabla\bar{T}, \end{array}\right\} \tag{4}$$

thus we have for the fluctuating quantities

$$\left.\begin{array}{l} \tilde{\boldsymbol{v}} = \dfrac{RP}{\omega M^2}\sin(\tau)\boldsymbol{u}, \\ \tilde{T} = \dfrac{RP}{\omega M^2}\cos(\tau)(\boldsymbol{u}\cdot\nabla\bar{T}), \end{array}\right\} \tag{5}$$

where the solenoidal vector $\boldsymbol{u}$ is the rotational part of the vector $\bar{T}\hat{\boldsymbol{n}}$, i.e.

$$\bar{T}\hat{\boldsymbol{n}} = \boldsymbol{u} + \nabla\phi, \tag{6}$$

for some higher-order scalar field ϕ associated with $\tilde{p}$. With the tilde variables determined, the equations for the mean field are

$$\left.\begin{aligned}
&\nabla\cdot\bar{\boldsymbol{v}} = 0,\\
&\frac{M}{P}\frac{\mathrm{D}\bar{\boldsymbol{v}}}{\mathrm{D}t} = -\nabla\bar{p} + \nabla^2\bar{\boldsymbol{v}} + G(\boldsymbol{u}\cdot\nabla)(\bar{T}\hat{\boldsymbol{n}} - \mathbf{u}),\\
&\nabla\cdot\boldsymbol{u} = 0,\\
&\nabla\times\bar{T}\hat{\boldsymbol{n}} = \nabla\times\boldsymbol{u} = \nabla\bar{T}\times\hat{\boldsymbol{n}},\\
&M\frac{\mathrm{D}\bar{T}}{\mathrm{D}t} = \nabla^2\bar{T},\\
&\bar{u} = \bar{v} = \bar{w} = \partial_z\bar{T} = 0 \qquad \text{on} \quad z = 0,\\
&\partial_z\bar{u} + \partial_x\bar{T} = \partial_z\bar{v} + \partial_y\bar{T} = \bar{w} = \partial_z\bar{T} = 0 \qquad \text{on} \quad z = 1,\\
&\bar{T} = -x \qquad \text{on} \quad z = 1.
\end{aligned}\right\} \tag{7}$$

where the vibrational parameter

$$G = \frac{R^2 P}{2M^3\omega^2}. \tag{8}$$

This inverse dependence of G on M^3 points to difficulties with this approach when $M = 0$ and will be discussed in § 4.2. The boundary conditions on the mean field are similar to those given by (2). Because the viscous terms drop out of (4*a*) at leading order, only the normal component of $\boldsymbol{u}$ can be made to vanish there.

In the absence of vibrations $G = 0$ the simple return flow possible is

$$\left.\begin{aligned}
&\bar{u} = U_s(z) = \tfrac{3}{4}z^2 - \tfrac{1}{2}z,\\
&\bar{T} = -x + MF_s(z), \quad F_s(z) = \left(-\tfrac{1}{12}(1-z^3) + \tfrac{1}{16}(1-z^4)\right).
\end{aligned}\right\} \tag{9}$$

It can be seen that the influence of modulation on the mean motion is through the term $G(\boldsymbol{u}\cdot\nabla)(\bar{T}\hat{\boldsymbol{n}} - \boldsymbol{u})$ in (7*b*) and its curl gives the vorticity source that simplifies to

$$-G\nabla\bar{T}\times\nabla(\hat{\boldsymbol{n}}\cdot\boldsymbol{u}),$$

and vanishes for some simple basic flows if $\hat{\boldsymbol{n}}\cdot\boldsymbol{u} = 0$. One of these is when the layer vibrates normal to its boundaries with $\hat{\boldsymbol{n}} = \hat{\boldsymbol{k}}$. In this case, the system (7) implies the same background state as (9) along with

$$\boldsymbol{u} = u_0(z)\hat{\mathbf{i}}, \qquad u_0(z) = z - 1/2, \qquad \text{so that} \quad \int_0^1 u_0(z)\,\mathrm{d}z = 0, \tag{10}$$

which completes evaluation of the fluctuating part of the basic flow in (5) when $G \neq 0$.

3.2. *Instability of the return flow*

Linear stability of the basic flow given by (9) and (10) is considered by assuming perturbations of the form $(p, u, v, w, \vartheta, f, g, h)(z)\exp(\mathrm{i}\alpha x + \mathrm{i}\beta y - \mathrm{i}st)$ in, respectively, $\bar{p}$, components of $\bar{\boldsymbol{v}}, \bar{T}$ and components of $\boldsymbol{u}$. Substitution in (7), linearization and

elimination of f and g leads to the eigenvalue problem

$$\left.\begin{aligned}
&\mathrm{i}\alpha u + \mathrm{i}\beta v + w' = 0,\\
&L_R u - RU_s' w - \mathrm{i}\alpha p - G\left(u_0' - \frac{\alpha^2}{\gamma^2}u_0\mathrm{D}\right)h = -\mathrm{i}sRu,\\
&L_R v - \mathrm{i}\beta p + G\frac{\alpha\beta}{\gamma^2}u_0 h' = -\mathrm{i}sRv,\\
&L_R w - p' + \mathrm{i}\alpha G u_0\vartheta + G\left(-\mathrm{i}\alpha u_0 + MF_s' - \frac{\mathrm{i}\alpha}{\gamma^2}\mathrm{D}\right)h = -\mathrm{i}sRw,\\
&L_M\vartheta + Mu - M^2F_s'w = -\mathrm{i}sM\vartheta,\\
&(\mathrm{D}^2 - \gamma^2)h + \gamma^2\vartheta = 0,\\
&u = v = w = \vartheta' = h = 0 \qquad \text{on} \quad z = 0,\\
&u' + \mathrm{i}\alpha\vartheta = v' + \mathrm{i}\beta\vartheta = w = \vartheta' = h = 0 \qquad \text{on} \quad z = 1.
\end{aligned}\right\} \tag{11}$$

where $\gamma^2 = \alpha^2 + \beta^2$, primes and D denote $\mathrm{d}/\mathrm{d}z$ and $L_R = \mathrm{D}^2 - \gamma^2 - \mathrm{i}\alpha RU_s$.

For each pair G and P, and for each pair α and β, M is calculated so that

$$\max(\mathrm{Im}\{s(M, \alpha, \beta; G, P)\}) = 0.$$

The critical Marangoni number M_c and the critical wavenumbers α_c and β_c are determined by minimization using the subroutine AMOEBA given by Press *et al.* (1986).

Solutions of (11) were found using the Chebyshev pseudospectral method and Lapack subroutines for solving the resulting algebraic eigenvalue problem of order $6N$, N being the number of basis functions in the representations of $(p, u, v, w, \vartheta, h)(z)$. $N \geqslant 20$ was typically employed in order to obtain converged results with at least two significant digits in the computed critical parameters.

3.3. *Numerical results*

Figure 1 displays the variation of M_c with G when $P = 0.01$. It is seen that vibrations, or gravity modulations, are stabilizing at high frequencies. The critical values $M_c = 6.292$, $\alpha_c = 0.0552$, $\beta_c = 0.236$ and $\mathrm{Re}(s_c) = -0.0177$ at $G = 0$ are in good agreement with those given by Smith & Davis (1983). As shown in figures 2 and 3, α_c, β_c and $\mathrm{Re}(s_c)$ exhibit weak dependence on G at this P. The critical frequency is negative, thus the waves continue to propagate against the free-surface flow in this range of G. The situation is markedly different at larger P. Corresponding plots at $P = 1$ and $P = 10$ are given in figures 4–6 and 7–9, respectively. With $P = 1$, figure 5 indicates small changes in β_c with G, while α_c first decreases to zero at $G = G_r = 6.68$ and then increases as a different eigensolution dominates. $\mathrm{Re}(s_c)$ is shown in figure 6 to first decrease from its negative value at $G = 0$. The preferred mode that emerges at $G \geqslant G_r$ is with $\mathrm{Re}(s_c) > 0$, thus signalling wave reversal. With $P = 10$ both α_c and β_c first decrease as shown in figure 8 until $G = G_r = 0.191$ where a transverse eigensolution with $\beta_c \approx 0$ is preferred. Figure 9 also confirms wave reversal for $G \geqslant G_r$. Figures 4 and 7 show that modulation at large P is also stabilizing at high frequencies. Finally, in figure 10, the dependence of G_r on P is given where it is seen that wave reversal occurs at very small G_r with increasing P and at very large G_r with decreasing P. Thus, calculation of G_r with $P = 0.01$ was not attempted.

The almost linear dependence of M_c on G shown in figure 1 with $P = 0.01$ is remarkable and is associated with long oblique waves. An asymptotic analysis in the limits $P \to 0$, $\alpha \to 0$, $\beta \to 0$ might reveal why this is so. Likewise, M_c increases almost linearly with G, for large G, at all the values of P in figures 1, 4 and 7.

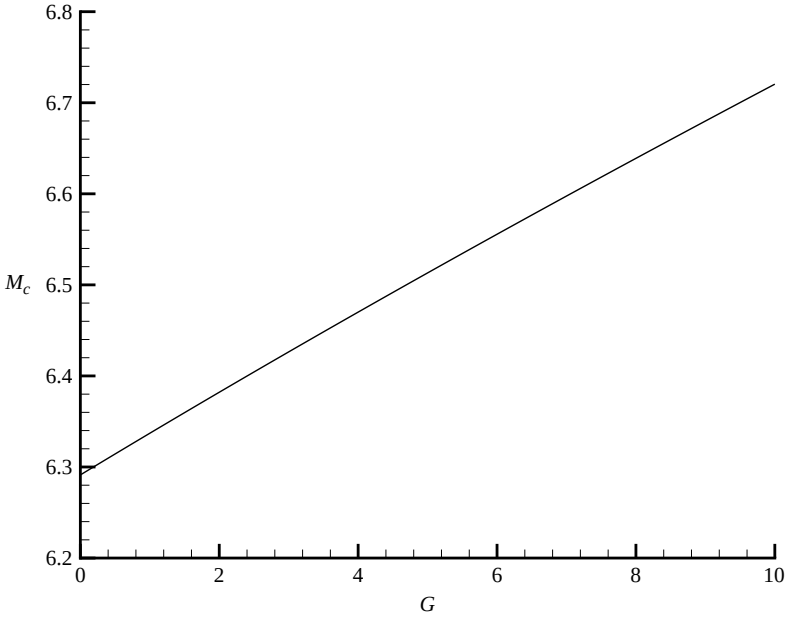

FIGURE 1. Variation of the critical Marangoni number M_c with the vibrational parameter G when the Prandtl number $P = 0.01$. The flow is unstable for $M > M_c$ thus modulation is stabilizing.

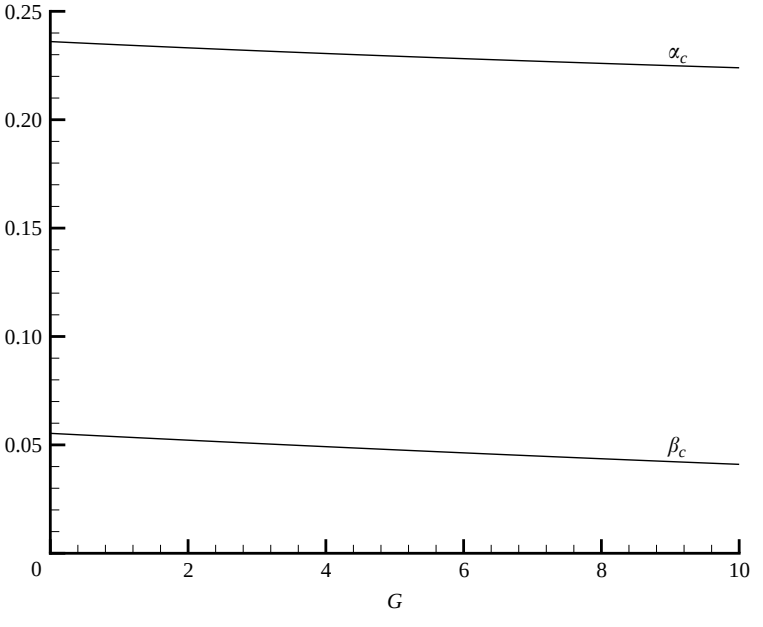

FIGURE 2. Variation of the critical wavenumbers α_c and β_c with G at $P = 0.01$. Almost the same values as with the pure hydrothermal waves at $G = 0$ prevail.

An asymptotic analysis in the limit $G \to \infty$ might be successful in explaining this dependence.

The above results pertain to the influence of modulation on the thermocapillary branch. For the values of P considered, we found no solutions that correspond to M

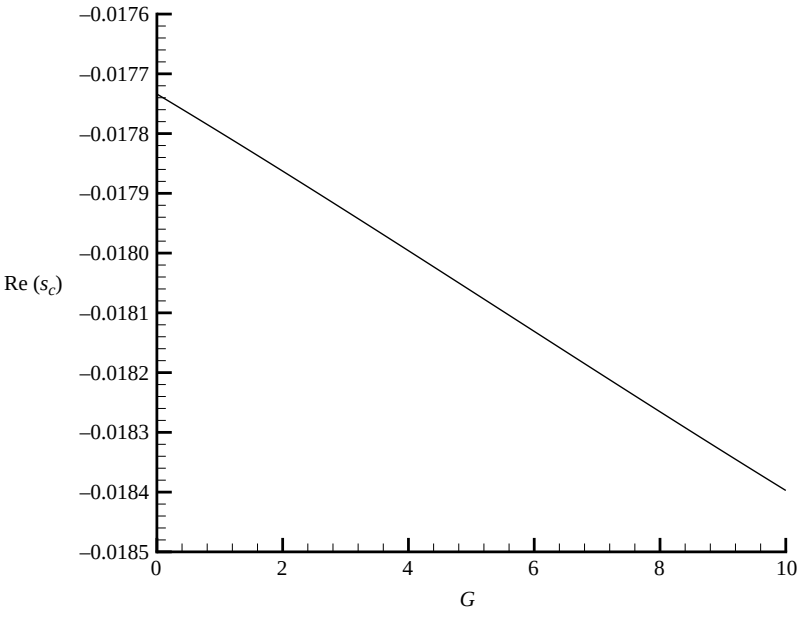

FIGURE 3. Variation of the critical frequency $Re(s_c)$ with$G$ at $P = 0.01$ shows small deviation from the pure hydrothermal waves at $G = 0$.

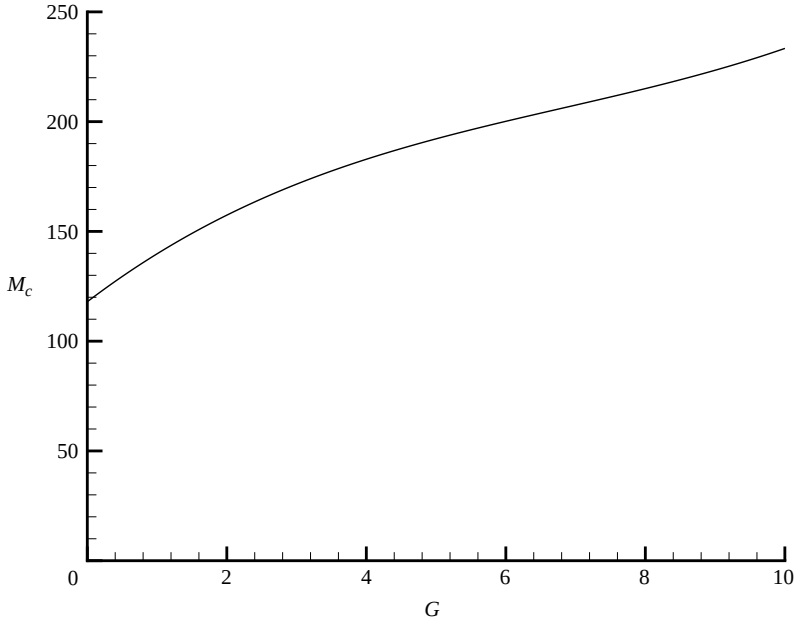

FIGURE 4. As figure 1, but with $P = 1$.

near zero or below M_c at $R = 0 (G = 0)$. Thus the high-frequency limit was not successful in providing information on the pure buoyant branch at $M = 0$ or the combined buoyant–thermocapillary instabilities at $M \approx 0$ that we study next by Floquet theory.

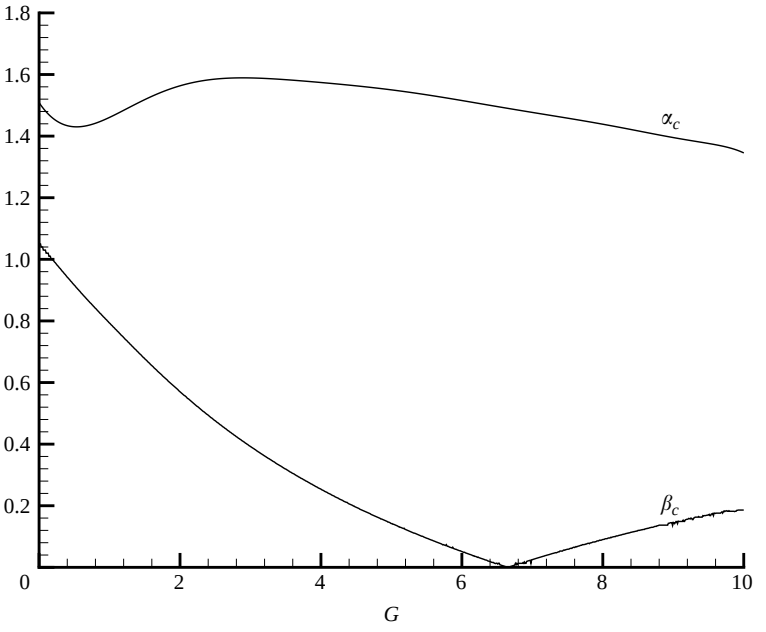

FIGURE 5. Variation of the critical wavenumbers α_c and β_c with G at $P = 1$. A different mode dominates at $G \geqslant G_r = 6.68$.

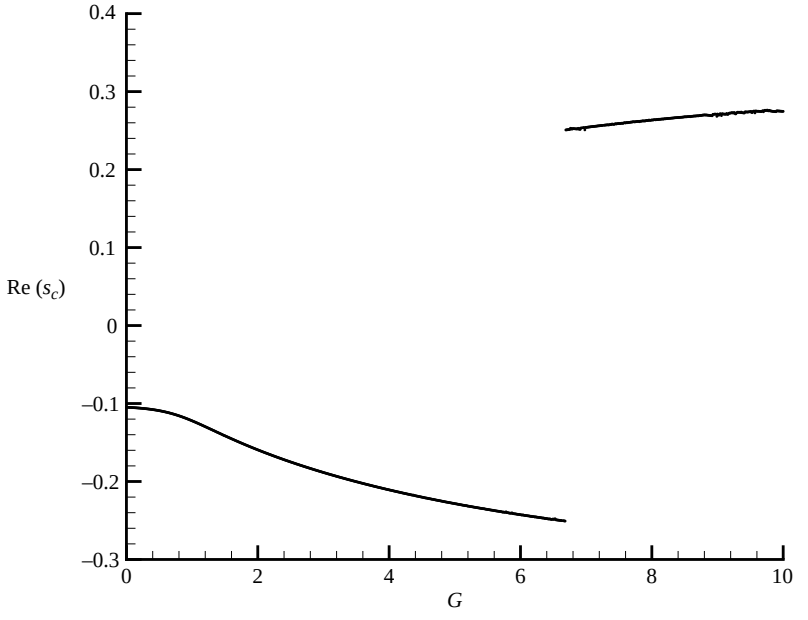

FIGURE 6. Variation of the critical frequency $\mathrm{Re}(s_c)$ with G at $P = 1$. The preferred eigensolution for $G \geqslant G_r = 6.68$ has a positive frequency and thus the waves propagate in the same direction as the free surface flow.

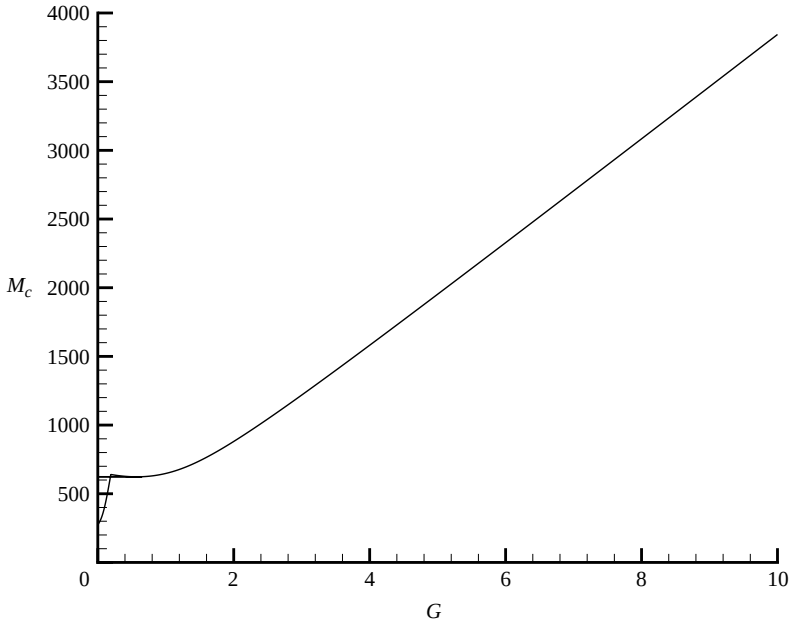

FIGURE 7. As figures 1 and 4, but with $P = 10$. There is a strong change of slope at $G = G_r = 0.191$.

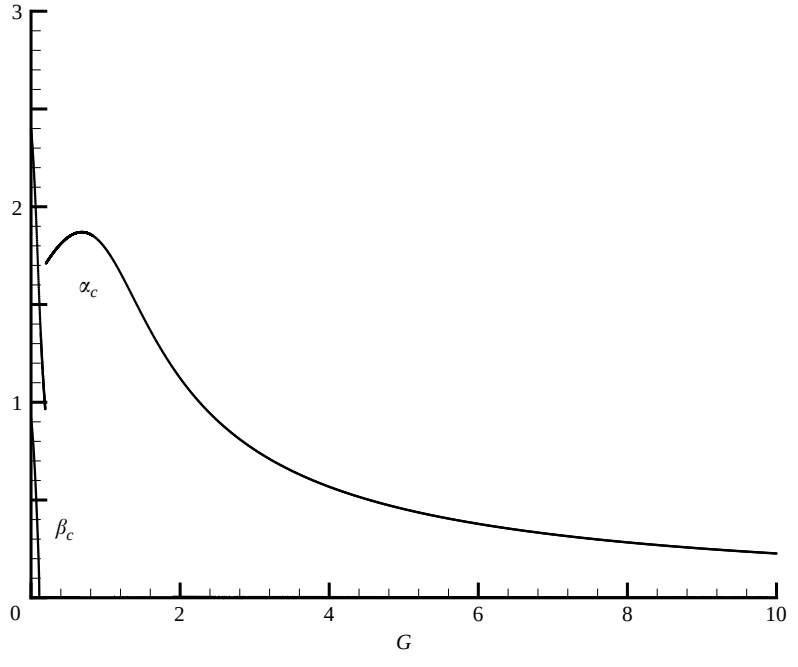

FIGURE 8. As figure 5, but with $P = 10$. A transverse critical mode with $\beta_c = 0$ emerges for $G \geqslant G_r$.

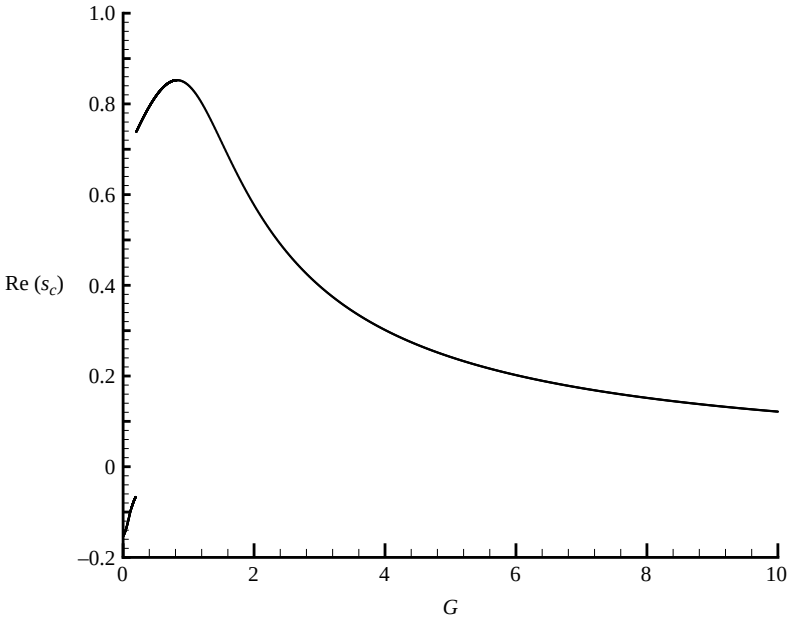

FIGURE 9. As figure 6 but with $P = 10$ and $G_r = 0.191$.

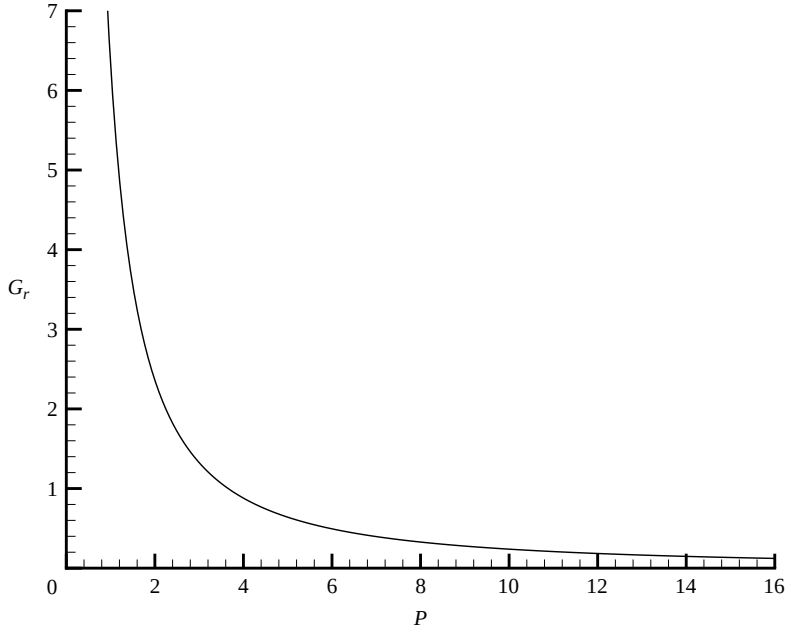

FIGURE 10. Variation of G_r with P.

4. Parametric instability

Here we consider instabilities at finite frequencies. In order to consider the case $M = 0$, we introduce the variables

$$t = \hat{t}/\omega, \quad \boldsymbol{v} = \hat{\boldsymbol{v}}/M, \quad p = \hat{p}/M, \quad T = \hat{T} \tag{12}$$

in (1) and (2) which is equivalent to choosing $1/\omega_1$ as time scale and κ/d as velocity scale as in SH. With $\Omega = M\omega = \omega_1 d^2/\kappa$, the governing system becomes

$$\left.\begin{aligned}
&\nabla\cdot\hat{\boldsymbol{v}} = 0,\\
&\frac{\Omega}{P}\frac{\partial\hat{\boldsymbol{v}}}{\partial\hat{t}} + \frac{1}{P}\hat{\boldsymbol{v}}\cdot\nabla\hat{\boldsymbol{v}} = -\nabla\hat{p} + \nabla^2\hat{\boldsymbol{v}} + R\hat{T}\cos(\hat{t})\hat{\boldsymbol{k}},\\
&\Omega\frac{\partial\hat{T}}{\partial\hat{t}} + \hat{\boldsymbol{v}}\cdot\nabla\hat{T} = \nabla^2\hat{T},\\
&\hat{u} = \hat{v} = \hat{w} = \partial_z\hat{T} = 0 \qquad \text{on } z = 0,\\
&\partial_z\hat{u} + M\partial_x\hat{T} = \partial_z\hat{v} + M\partial_y\hat{T} = \hat{w} = \partial_z\hat{T} = 0 \qquad \text{on } z = 1,\\
&\hat{T} = -x \qquad \text{on } z = 1.
\end{aligned}\right\} \tag{13}$$

System (13) admits the time-harmonic basic flow

$$\left.\begin{aligned}
&\hat{u} = U(z,\hat{t}) = MU_s(z) + R\mathrm{Re}\{U_a(z)\mathrm{e}^{\mathrm{i}\hat{t}}\},\\
&\hat{T} = -x + F(z,\hat{t}) = -x + MF_s(z) + R\mathrm{Re}\{F_a(z)\mathrm{e}^{\mathrm{i}\hat{t}}\},
\end{aligned}\right\} \tag{14}$$

where $U_s(z)$ and $F_s(z)$ are given in (9) and $U_a(z)$ and $F_a(z)$ satisfy

$$\left.\begin{aligned}
&\frac{\mathrm{i}\Omega}{P}U_a' = U_a''' + 1,\\
&\mathrm{i}\Omega F_a - U_a = F_a'',\\
&U_a(0) = F_a'(0) = U_a'(1) = F_a'(1) = \int_0^1 U_a\,\mathrm{d}z = 0.
\end{aligned}\right\} \tag{15}$$

The solution of (15) is given by

$$\left.\begin{aligned}
U_a &= \frac{z}{a^2} + c_1\mathrm{e}^{az} + c_2\mathrm{e}^{-az} + c_3,\\
F_a &= \frac{z}{a^2b^2} + b_1\mathrm{e}^{bz} + b_2\mathrm{e}^{-bz} + b_3\mathrm{e}^{az} + b_4\mathrm{e}^{-az} + b_5, \qquad P \neq 1,\\
F_a &= \frac{z}{a^4} + (d_1 + d_3z)\mathrm{e}^{az} + (d_2 + d_4z)\mathrm{e}^{-az} + d_5, \qquad P = 1,
\end{aligned}\right\} \tag{16}$$

where $a = \sqrt{\mathrm{i}\Omega/P}$, $b = \sqrt{\mathrm{i}\Omega}$, and the constants of integration are given in the Appendix. The properties of this oscillatory return flow were thoroughly discussed by SH. They pointed out that buoyant stable and unstable stratifications occur within a cycle. Thus the flow can be destabilized even at $M = 0$.

4.1. *Floquet analysis*

Instability of the basic flow in (14) is explored, assuming perturbations of the form $(p, u, v, w, \vartheta)(z,\hat{t})\exp(\mathrm{i}\alpha x + \mathrm{i}\beta y)$ in, respectively, $\hat{p}$, components of $\hat{\boldsymbol{v}}$ and

$\widehat{T}$. Substituting in (13), linearizing, and eliminating p and u yields

$$\left.\begin{aligned}
&\frac{\gamma^2\Omega}{\alpha^2 P}\mathrm{D}\dot{v} - \frac{\mathrm{i}\beta\Omega}{\alpha^2 P}\mathrm{D}\dot{w} = \frac{\gamma^2}{\alpha^2}(\mathrm{D}^2-\gamma^2)v - \frac{\mathrm{i}\gamma^2}{\alpha P}Uv \\
&\qquad\qquad - \frac{\mathrm{i}\beta}{\alpha^2}(\mathrm{D}^2-\gamma^2)\mathrm{D}w + \frac{\beta}{\alpha P}(\mathrm{D}U - U\mathrm{D})w, \\
&-\frac{\mathrm{i}\beta\Omega}{\alpha^2 P}\mathrm{D}\dot{v} + \frac{\Omega}{P}\left(1-\frac{\mathrm{D}^2}{\alpha^2}\right)\dot{w} = -\frac{\beta}{\alpha P}\mathrm{D}(Uv) - \frac{\mathrm{i}\beta}{\alpha^2}(\mathrm{D}^2-\gamma^2)\mathrm{D}v \\
&\qquad\qquad + \frac{\mathrm{i}}{\alpha P}(U\mathrm{D}^2 - \mathrm{D}^2U)w - \frac{\mathrm{i}}{\alpha P}Uw \\
&\qquad\qquad + (\mathrm{D}^2-\gamma^2)\left(1-\frac{\mathrm{D}^2}{\alpha^2}\right)w + R\cos(\widehat{t})\vartheta, \\
&\Omega\dot{\vartheta} = (\mathrm{D}^2 - \gamma^2 - \mathrm{i}\alpha U)\vartheta - \frac{\beta}{\alpha}v + \frac{\mathrm{i}}{\alpha}\mathrm{D}w - \mathrm{D}F w, \\
&v = w = \mathrm{D}w = \mathrm{D}\vartheta = 0 \qquad\qquad \text{on} \quad z = 0, \\
&\mathrm{D}v + \mathrm{i}\beta M\vartheta = w = \mathrm{D}^2 w + \gamma^2 M\vartheta = \mathrm{D}\vartheta = 0 \qquad \text{on} \quad z = 1.
\end{aligned}\right\} \tag{17}$$

Psudospectral Chebyshev z-decomposition of $(v, w, \vartheta)(z, \widehat{t})$ results in an ordinary initial-value problem of the form

$$\dot{\boldsymbol{\chi}} = \boldsymbol{A}\boldsymbol{\chi}, \qquad \boldsymbol{A}(\widehat{t} + 2\pi) = \boldsymbol{A}(\widehat{t}), \tag{18}$$

where the vector $\chi(\widehat{t})$ is composed of the spectral coefficients. Floquet theory (Glendinning 1994) states that the fundamental matrix solution $\Phi(t)$ of (18) with $\Phi(0) = I$ satisfies $\Phi(\widehat{t}+2\pi) = \Phi(\widehat{t})\Phi(2\pi)$. Thus if $\lambda_i, i = 1, \ldots, 3N$, N being the number of basis functions, are the eigenvalues of $\Phi(2\pi)$ then the Floquet exponents ε_i are given by

$$\varepsilon_i = \frac{1}{2\pi}\log(\lambda_i).$$

For each pair R and P, and for each pair α and β, M is calculated so that

$$\max(\mathrm{Re}\{\varepsilon(M, \alpha, \beta; R, P)\}) = 0.$$

The critical Marangoni number M_c and the critical wavenumbers α_c and β_c are determined by minimization in the (α, β)-plane. Likewise, the process is repeated for every pair M and P, and for each pair α and β, R is calculated so that

$$\max(\mathrm{Re}\{\varepsilon(R, \alpha, \beta; M, P)\}) = 0,$$

followed by minimization to calculate the critical point. In this way, we produce two stability branches emanating, respectively, from $R = 0$ and $M = 0$.

Up to $N = 26$ basis functions were employed in order to obtain good accuracy. As few as 18 were typically sufficient with larger N required for calculations at large Ω, R and P. Integration of (18) to evaluate $\Phi(2\pi)$ with $\Phi(0) = I$ was accomplished using the subroutine DASSL which is suitable for differential/algebraic stiff problems and is available from http://netlib.org/ode/index.html.

The imaginary part of ε_i characterizes the type of asymptotic instability; subharmonic if integer multiple of 1/2, synchronous if integer including zero, and quasi-periodic if the Floquet exponents are complex conjugate pairs incommensurate with modulation. While all these modes are generally present in the spectrum, we found all the preferred modes quasi-periodic, except for the pure buoyant instabilities with $M = 0$ where they are synchronous.

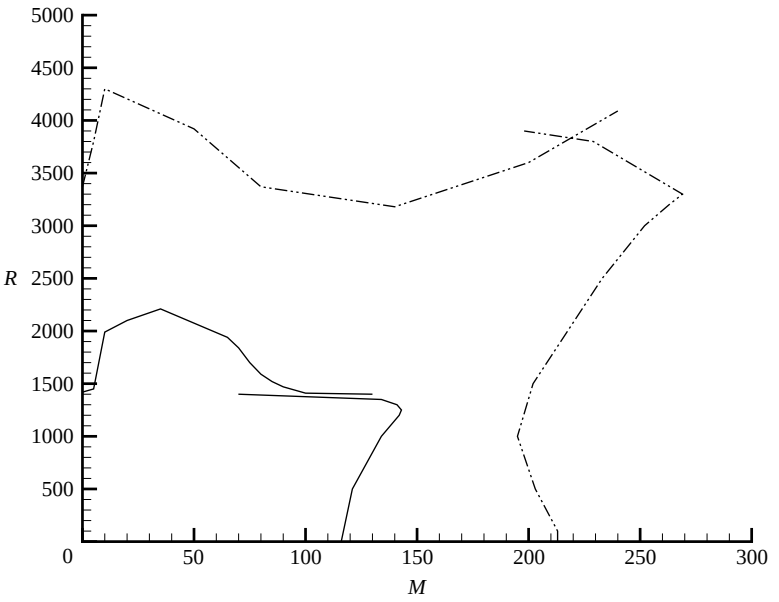

FIGURE 11. Stability boundaries in the (R, M)-plane when $P = 1$ and $\Omega = 10$. Critical thermocapillary or buoyant waves are three-dimensional. Preferred waves triggered by both mechanisms are also three-dimensional —, three-dimensional; –··–, two-dimensional.

4.2. *Numerical results with* $P = 1$

Figure 11 displays the two- and three-dimensional critical curves (calculations were performed for sufficiently small increments in either M or R) corresponding to $\Omega = 10$. When $R = 0$, we recover the results of Smith & Davis (1983) with the oblique three-dimensional waves preferred and good agreement in the values of M_c. When $M = 0$, our value for the two-dimensional R_c is in good agreement with SH. Some qualitative and/or quantitative agreement are also obtained with regards to the influence of $M(R)$ on the two-dimensional $R_c(M_c)$. Three-dimensional instabilities are seen to be more critical everywhere in the (M, R) plane. While a small amplitude modulation destabilizes the two-dimensional hydrothermal waves, it stabilizes the preferred three-dimensional modes. Small thermocapillarity $M \leqslant 10$ and $M \leqslant 35$ seems to respectively stabilize both the purely buoyant two- and three-dimensional modes at this small value of Ω.

Three-dimensional modes continue to be preferred with increasing Ω as shown in figures 12 and 13 for $\Omega = 100$ and 200. Moreover, this large-frequency modulation stabilizes the hydrothermal waves, in qualitative agreement with the results of § 3.3. It also stabilizes the two-dimensional thermocapillary waves in contrast with figure 11 at $\Omega = 10$. While thermocapillarity continues to stabilize the purely three-dimensional buoyant instability up to $\Omega = 200$, calculations with larger Ω confirmed that it begins to destabilize it for $\Omega > 200$.

Results for several values of Ω are given in figure 14 with only the preferred three-dimensional modes included. As expected, all the hydrothermal waves originate at the same M_c with $R = 0$. It is observed that the overall region of stability grows with increasing Ω, and without bound along the R-axis. This would explain why the two time-scale analysis of § 3.1 failed to provide information on the upper buoyant branch in the limit $\Omega \to \infty$. Consider, for example, the case when $P = 1$, $\Omega = 200$, $M = 5$

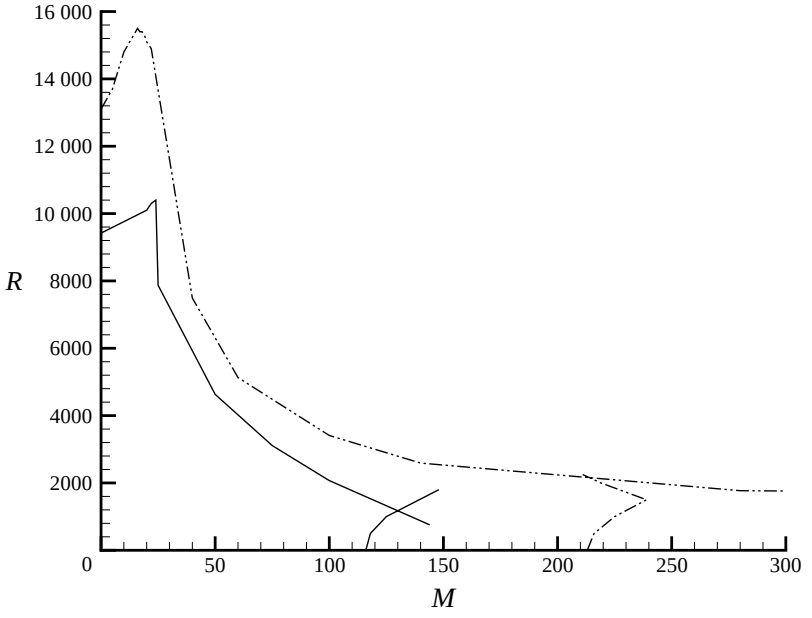

FIGURE 12. As figure 11, but with $\Omega = 100$.

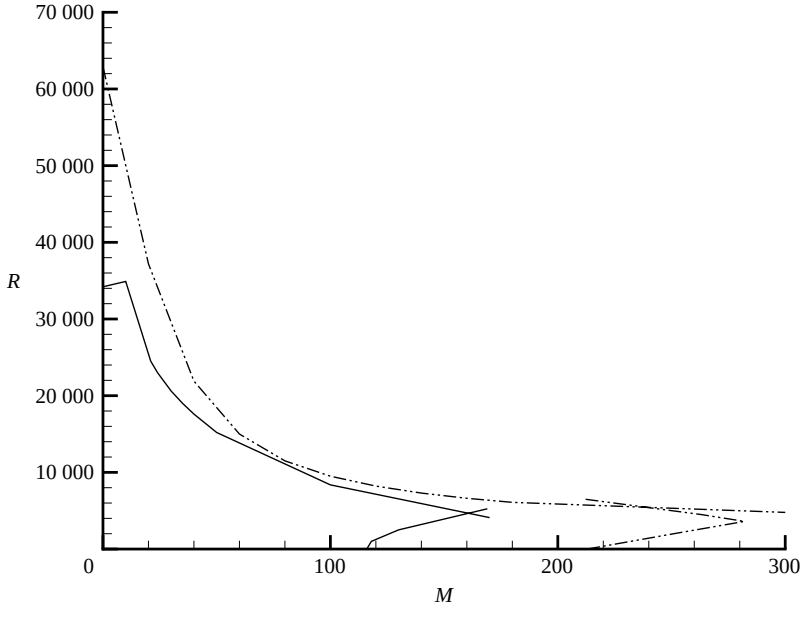

FIGURE 13. As figures 11 and 12, but with $\Omega = 200$. It is observed that the region of stability gets larger with increasing Ω.

with the three-dimensional $R = 34\,348$ from figure 14. It would require the asymptotic theory to be valid for $G = 2950$. Computationally, no solutions were found at such large G and yet larger values of G are associated with the buoyant branch at larger values of Ω.

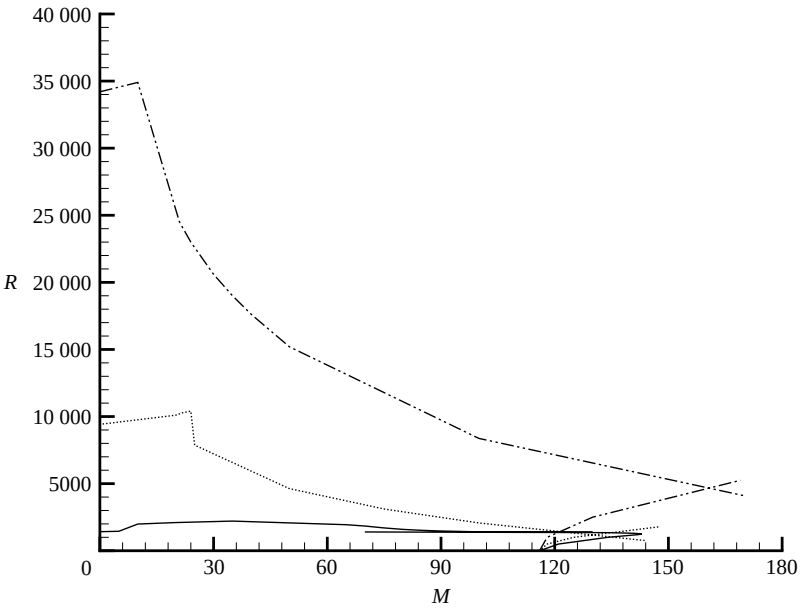

FIGURE 14. Stability boundaries of three-dimensional waves in the (R, M)-plane when $P = 1$ and —, $\Omega = 10, \ldots, 100$ and –·–, 200. The hydrothermal waves with $R = 0$ emanate from the Smith & Davis (1983) value of 116.02. The critical R for pure buoyant instabilities with $M = 0$ grows without bound as Ω increases, thus the region of stability also grows.

As observed earlier, there were no asymptotic solutions below $M < M_c(R = 0)$ as shown in figures 1, 4 and 7. Thus, the pure buoyant branch is not amenable to analysis in the high-frequency limit until $M > M_c(R = 0)$ where the buoyant-modified hydrothermal waves dominate.

4.3. *Other values of P*

Figure 15 gives the stability boundaries corresponding to $P = 0.01$ and $\Omega = 10$. In this case there are no two-dimensional thermocapillary waves with $R = 0$ in agreement with Smith & Davis (1983). The two-dimensional branch emanating from $\Omega > 200$ is in good agreement with SH. It is observed that the preferred region of three-dimensional stability is very small compared with the two-dimensional solutions. Modulation stabilizes the hydrothermal waves and thermocapillarity stabilizes the purely buoyant modes as it also does the two-dimensional branch. SH showed by energy analysis that the two-dimensional buoyant branch is strongly stabilized by shear at this small $P = 0.01$. This continues to be the case for the three-dimensional modes with $R_c(M = 0, P = 0.01, \Omega = 10)$ larger than $R_c(M = 0, P = 1, \Omega = 10)$ from figure 11.

Figure 16 with $P = 10$ and $\Omega = 10$ displays other possibilities. Thermocapilarity destabilizes (stabilizes) the two-(three-)dimensional buoyant modes. Modulation, however, initially stabilizes both two- and three-dimensional thermocapillary waves with the effect alternating with increasing R. In this case both two- and three-dimensional modes are such that $R_c(M = 0, P = 10, \Omega = 10)$ is larger than $R_c(M = 0, P = 1, \Omega = 10)$. This is in complete agreement with SH who explain the lowest threshold of instability at $P \approx 1$, not through the dynamics of the instability, but as a consequence of the properties of the underlying modulated base flow with weak unstable stratification resulting at small and large values of P.

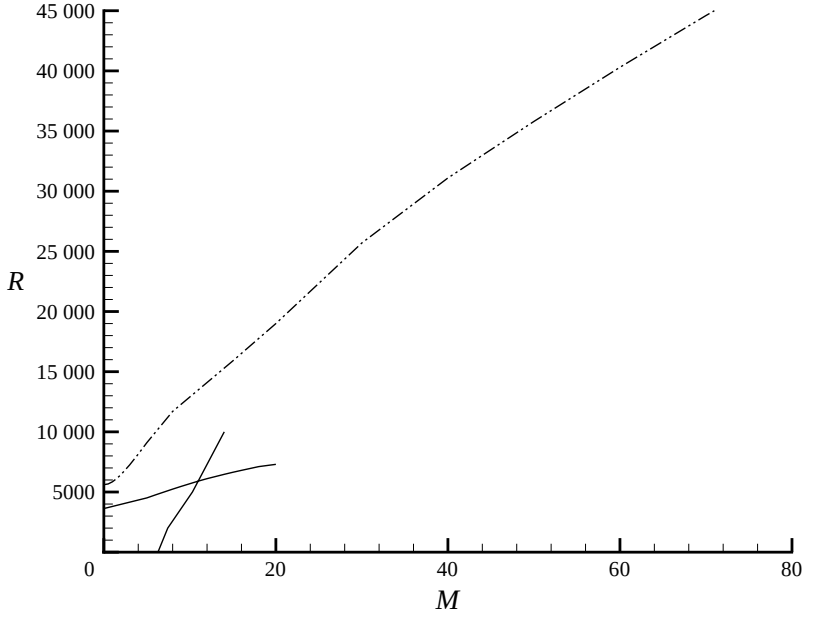

FIGURE 15. Stability boundaries in the (R, M)-plane when $P = 0.01$ and $\Omega = 10$. There is no two-dimensional thermocapillary branch. —, three-dimensional; –··–, two-dimensional.

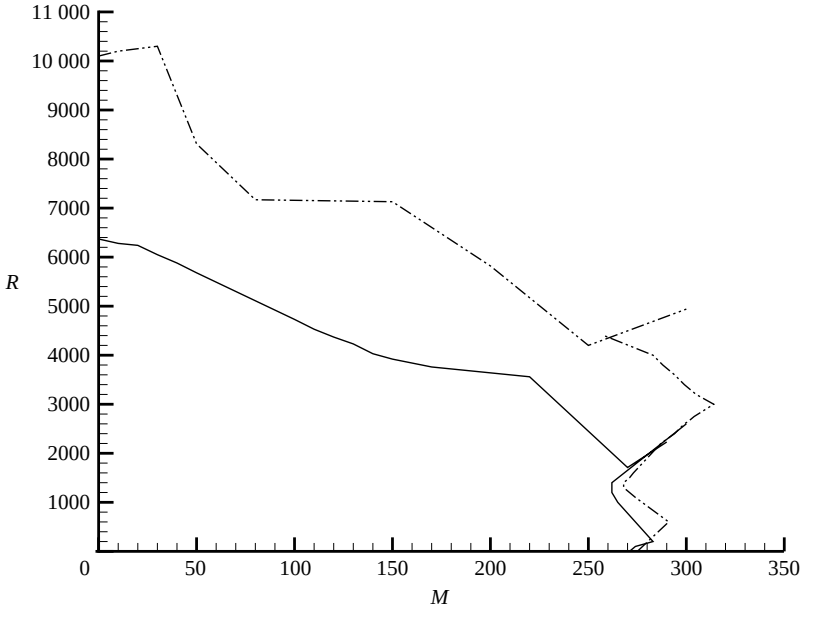

FIGURE 16. Stability boundaries in the (R, M)-plane when $P = 10$ and $\Omega = 10$. Figures 11, 15 and 16 display different patterns of the influence of $R(M)$ on the thermocapillary (buoyant) branches. —, three-dimensional; –··–, two-dimensional.

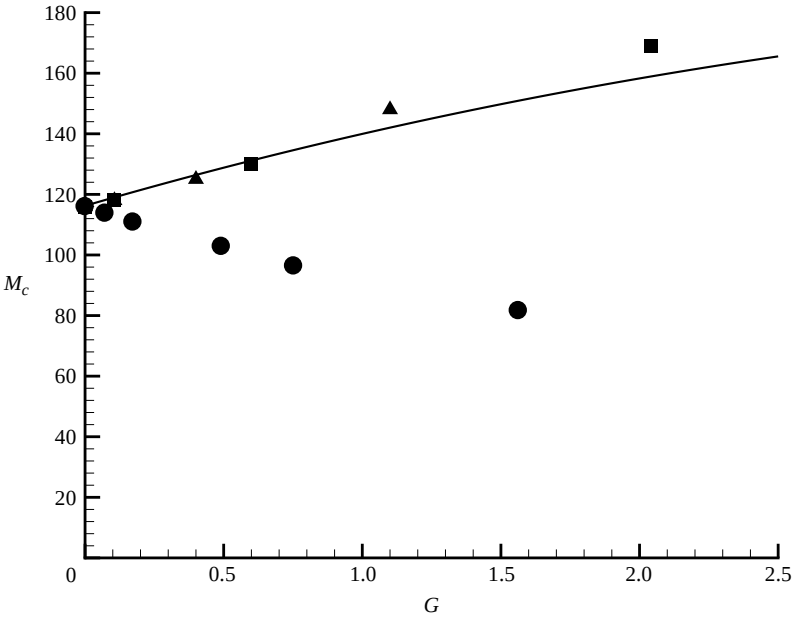

FIGURE 17. Comparison of —, the asymptotic and Floquet results. The variation of M_c with G corresponding to $P=1$ and ●, $\Omega=50$; ▲, 100; and ■, 200 is shown. Good agreement is obtained for $G<1$ and $\Omega \geqslant 100$.

4.4. *Large frequencies*

We first observe that in the limit $\Omega = M\omega \to \infty$ the alternating part of the basic flow in (14) given by (16) and (A 1)–(A 3) has the asymptotic form

$$\left.\begin{aligned}
R\mathrm{Re}\{U_a(z)\mathrm{e}^{\mathrm{i}\hat{t}}\} &\sim \frac{RP}{\Omega}(z-1/2)\sin(\hat{t}) \\
&\quad + \Omega^{-1}O\left(\Omega^{-1/2}\exp\left(-\sqrt{\frac{\Omega}{2P}}(1-z)\right),\ \exp\left(-\sqrt{\frac{\Omega}{2P}}z\right)\right), \\
R\mathrm{Re}\{F_a(z)\mathrm{e}^{\mathrm{i}\hat{t}}\} &\sim -\frac{RP}{\Omega^2}(z-1/2)\cos(\hat{t}) \\
&\quad + \Omega^{-2}O\left(\Omega^{-1/2}\exp\left(-\sqrt{\frac{\Omega}{2P}(1-z)}\right),\ \exp\left(-\sqrt{\frac{\Omega}{2P}}z\right),\right. \\
&\quad \left.\Omega^{-1/2}\exp\left(-\sqrt{\frac{\Omega}{2}(1-z)}\right),\ \exp\left(-\sqrt{\frac{\Omega}{2}}z\right)\right), \quad P\neq 1, \\
R\mathrm{Re}\{F_a(z)\mathrm{e}^{\mathrm{i}\hat{t}}\} &\sim -\frac{RP}{\Omega^2}(z-1/2)\cos(\hat{t}+\Omega^{-3/2}O\left(\Omega^{-1/2}\exp\left(-\sqrt{\frac{\Omega}{2}}(1-z)\right),\right. \\
&\quad \left.\exp\left(-\sqrt{\frac{\Omega}{2}}z\right)\right), \quad P=1,
\end{aligned}\right\} \tag{19}$$

and the leading part when written in terms of the tilde variables through the transformation (12) is precisely the leading fluctuating component of the basic flow given by (3), (5), (9) and (10). Equation (19) shows that agreement is reached outside the boundary layers of thickness $\sqrt{\Omega}$ at $z=0$ and $z=1$. Moreover larger values the Ω are required to reach the asymptotic regime at larger values of P.

Thus with increasing frequencies we expect the results of Floquet analysis in § 4 to agree with those from the high-frequency asymptotics in § 3. Figure 17 shows that this

is indeed the case. With $P=1$, we plot M_c against $G=R^2P/2M^3\omega^2=R^2P/2M\Omega^2$ at several values of Ω. The asymptotic result from figure 4 is also included. It is evident that must Ω exceed 100 with $P=1$ in order to achieve good agreement between the two instability theories for $G\leqslant 1$. Larger values of Ω are also required for agreement at larger values of G. Computations of the Floquet exponent at $G_r=6.68$ with $M=205.4$ from figure 4 requires solutions with $R=52.4\Omega$ at very large values of Ω and was computationally prohibitive.

Larger values of the Prandtl number required yet larger values of Ω in order for the Floquet results to agree with the asymptotic behavior. This is in agreement with (19) and similar to the findings of Wheeler *et al.* (1991) at high Schmidt numbers.

5. Discussion and conclusions

We have presented a reasonably complete study of the influence of vibrations, or equivalently zero mean gravity modulation, on thermocapillary instabilities. Three-dimensional modes are preferred everywhere in the (R, M)-plane. Floquet analysis provided information on finite frequencies, while two-time scale asymptotics provided results at large frequencies. Both approaches are in agreement asymptotically. Calculations of the Floquet exponents become very demanding with increasing frequencies and Prandtl numbers. Results from the asymptotic theory become invaluable at these extremes. In particular, wave reversal which is predicted by the asymptotic results, could not be ascertained by Floquet analysis and awaits experimental validation.

Pure buoyant instabilities with $M=0$ are triggered with $R\to\infty$ as $\Omega\to\infty$. This is expected as these instabilities are driven in the unstably stratified part of the cycle that shrinks to zero in this limit. Thus this branch could not be investigated in the high-frequency limit. The critical R for these instabilities is least when $P=1$. With $P=1$ and at low frequencies the flow is stabilized, destabilized, and then stabilized as M increases from zero. At high frequencies, thermocapillarity destabilizes this branch for all $M>0$.

With $P\leqslant 1$, modulation stabilizes the three-dimensional thermocapillary branch for all $R>0$ and all frequencies. At the larger $P=10$ and at low frequencies, there are regions of alternating stability and instability as R increases from zero. At high frequencies, modulation stabilizes the thermocapillary branch for any value of P.

The results of the present paper can also be useful for understanding thermocapillary instabilities in a microgravity environment with g-jitter (Wheeler *et al.* 1991; Zebib 2001) where typical values of Ω exceed 100.

Appendix

The constants of integration associated with the alternating component of the return flow in (16) are:

$$\left.\begin{aligned} c_1 &= \left(\frac{\{e^{-a}(1-a^2/2)+a-1)\}}{2a^3\{\sinh(a)-a\cosh(a)\}}\right),\\ c_2 &= \left(\frac{\{e^{a}(1-a^2/2)-a-1)\}}{2a^3\{\sinh(a)-a\cosh(a)\}}\right),\\ c_3 &= -c_1-c_2, \end{aligned}\right\} \tag{A 1}$$

$$\left.\begin{aligned} d_1 &= \frac{1}{4a\sinh(a)}\left(c_2\mathrm{e}^{-a} + c_1\mathrm{e}^{a} + \frac{2\sinh(a)c_1}{a} + \frac{2(\mathrm{e}^{-a}-1)}{a^4}\right), \\ d_2 &= \frac{1}{4a\sinh(a)}\left(c_2\mathrm{e}^{-a} + c_1\mathrm{e}^{a} + \frac{2\sinh(a)c_2}{a} + \frac{2(\mathrm{e}^{a}-1)}{a^4}\right), \\ d_3 &= \frac{-c_1}{2a}, \quad d_4 = \frac{c_2}{2a}, \quad d_5 = \frac{c_3}{a^2}, \end{aligned}\right\} \tag{A 2}$$

$$\left.\begin{aligned} b_1 &= \frac{1}{2b\sinh(b)}\left(\frac{-a(c_2-c_1)\mathrm{e}^{-b}}{b^2-a^2} + \frac{a(c_2\mathrm{e}^{-a}-c_1\mathrm{e}^{a})}{b^2-a^2} + \frac{(\mathrm{e}^{-b}-1)}{a^2b^2}\right), \\ b_2 &= \frac{1}{2b\sinh(b)}\left(\frac{-a(c_2-c_1)\mathrm{e}^{b}}{b^2-a^2} + \frac{a(c_2\mathrm{e}^{-a}-c_1\mathrm{e}^{a})}{b^2-a^2} + \frac{(\mathrm{e}^{b}-1)}{a^2b^2}\right), \\ b_3 &= \frac{c_1}{b^2-a^2}, \quad b_4 = \frac{c_2}{b^2-a^2}, \quad b_5 = \frac{c_3}{b^2}. \end{aligned}\right\} \tag{A 3}$$

REFERENCES

Birikh, R. V. 1966 Thermocapillary convection in a horizontal fluid layer. *J. Appl. Mech. Tech. Phys.* **7**, 43.

Chen, W.-Y. & Chen, C. F. 1999 Effect of gravity modulation on the stability of convection in a vertical slot. *J. Fluid Mech.* **395**, 327–344.

Farooq, A. & Homsy, G. M. 1996 Linear and nonlinear dynamics of a differentially heated slot under gravity modulation effect. *J. Fluid Mech.* **313**, 1–38.

Gershuni, G. Z., Kolesnikov, A. K., Legros, J.-C. & Myznikova, B. I. 1997 On the vibrational convective instability of a horizontal, binary-mixture layer with Soret effect. *J. Fluid Mech.* **330**, 251–269.

Gershuni, G. Z. & Zhukhovitskii, E. M. 1976 *Convective Stability of Incompressible Fluids*. Keter Publishing House Jerusalem.

Glendinning, P. 1994 *Stability, Instability and Chaos: an Introduction to the Theory of Nonlinear Differential Equations*, pp. 70–73. Cambridge University Press.

Gresho, P. M. & Sani, R. L. 1970 The effects of gravity modulation on the stability of a heated fluid layer. *J. Fluid Mech.* **40**, 783–806.

Murray, B. T., Coriell, S. R., McFadden, G. B., Wheeler, A. A. & Saunders, B. V. 1993 Gravitational modulation of thermosolutal convection during directional solidification. *J. Cryst. Growth* **129**, 70–80.

Press, W. H., Flannery, B. P., Teukolsky, S. A. & Vetterling, W. T. 1986 *Numerical Recipes*. pp. 292–293, Cambridge University Press.

Smith, M. K. & Davis, S. H. 1983 Instabilities of dynamic thermocapillary liquid layers. Part 1. Convective instabilities. *J. Fluid Mech.* **132**, 119–144.

Suresh, V. & Homsy, G. M. 2001 Stability of return thermocapillary flows under gravity modulation. *Phys. Fluids* **13**, 3155–3167.

Wheeler, A. A., McFadden, G. B., Murray, B. T. & Coriell, S. R. 1991 Convective stability in the Rayleigh–Bénard and directional solidification problems: high frequency gravity modulation. *Phys. Fluids* A **3**, 2847–2858.

Zebib, A. 2001 Low-gravity sideways double-diffusive instabilities. *Phys. Fluids* **13**, 1829–1832.